Support Information

Rational Element-doping of FeOOH-based electrocatalysts for Efficient Ammonia Electrosynthesis

Haifan Wang[1,2,3], Menglei Yuan[1,4]*, Jingxian Zhang[1,2], Yiling Bai,[5,6] Ke Zhang[7], Bin Li[7]*, Guangjin Zhang[1,2]*

[1] CAS Key Laboratory of Green Process and Engineering, Institute of Process Engineering, Chinese Academy of Sciences, Beijing 100190, China

[2] Center of Materials Science and Optoelectronics Engineering, University of Chinese Academy of Sciences, Beijing 100049, China

[3] School of Chemical Engineering, University of Chinese Academy of Sciences, Beijing 100049, China

[4] Northwestern Polytechnical University, Xian 710000, China

[5] CAS Key Laboratory of Carbon Materials, Institute of Coal Chemistry, Chinese Academy of Sciences, Taiyuan 030001, China

[6] SynCat@Beijing, Synfuels China Technology Co. Ltd, Beijing 101407, China

[7] Zhengzhou Tobacco Research Institute of CNTC, Zhengzhou 450001, China

E-mail addresses: lib@ztri.com.cn and zhanggj@ipe.ac.cn

Characterization

X-ray diffraction (XRD, X'PERT PRO MPD diffractometer, Cu Kα radiation, λ=0.15418 nm, scanned range of 2 - 90°) was used to identify the crystal structure of all prepared catalysts. Scanning electron microscopy (SEM, JSM-7800F Prime) and transmission electron microscopy (TEM, JEM-2100F) were utilized to investigate the morphology of all samples. The Raman measurements were carried out on a Renishaw Raman Test system (λ = 532 nm). Temperature programmed desorption (TPD) were recorded on the AutoChem II2920. X-ray photoelectron spectroscopy (XPS) data were collected by using Krato, AXIS-HS monochromatized Al Kα cathode source of 75-150 W under ultrahigh vacuum. Fourier Transform Infrared Spectrometer (FTIR) and the spin state of the catalysts were tested on NICOLET Is 50 (Thermo) and MPMS-3 (Quantum Design), respectively. Moreover, the UV-visible adsorption spectra was recorded on a spectrophotometer (UV-2550). ^{1}H NMR spectra was collected on a superconducting-magnet NMR spectrometer (Bruker AVANCE III HD 700 MHz).

Electrochemical measurements

All electrochemical characterizations were performed using an electrochemical workstation CHI660E coupled with a three-electrode system in a H-type electrochemical reaction cell separated by Nafion 211 membrane. And the Nafion membrane was treated by boiling in ultrapure water for 1 h and heated in H_2O_2 (5 %) aqueous solution at 80 ℃ for another 1 h. Carbon cloth utilized in this work was purchased from CeTech (W1S1009 type) and treated with the mixture of H_2SO_4 and H_2O_2 (1:3 vol.) for 12 h to remove surface impurities.

Potential without iR-compensated was converted to RHE scale via the following equation: E (vs. RHE) = E (vs. Ag/AgCl) + 0.0591 × pH + 0.197. All experiments were carried out at room temperature (25 ℃). To remove the impurities in the inlet gas, such as NO_x, the pre-purification of high-purity N_2 (purity 99.999 %) and Ar (purity 99.999 %) by passing through two saturators filled with 0.05 M NaOH and 0.05 M H_2SO_4 solution, respectively, to remove any possible contaminants. Then, the

electrolyte solution was purged with the purified raw gas (N_2, Ar) for 30 minutes at a rate of 30 sccm in 0.1 M $LiClO_4$ + 20 % PEG.

Cyclic voltammetry (CV) test for activating the electrode was carried out at a scan rate of 50 mV s^{-1} ranging from 0 to -1.0 V vs. RHE. Linear sweep voltammetry (LSV) was also conducted at a scan rate of 5 mV s^{-1} ranging from 0 to -1.0V vs. RHE. Chronoamperometric tests were then conducted at different potentials (-0.4 - -0.8 V vs. RHE) and N_2 was continuously fed into the cathodic cell during the experiments. The recycle test was to perform five consecutive cycles of chronoamperometric tests without changing the electrolyte at -0.6 V vs. RHE. Electrochemical impedance spectroscopy (EIS) was conducted at a frequency range from 100 kHz to 1 Hz with a 10 mV AC signal amplitude.

Determination of NH_3 concentration by indophenol blue method[1]

When tested in 0.1 M $LiClO_4$ and 0.1 M $LiClO_4$ + 20 % PEG, the produced NH_3 was spectrophotometrically determined by the indophenol blue method. Typically, 2 mL of the sample solution was removed from the cathodic chamber. Afterward, 2 mL of 1.0 M NaOH solution containing 5 wt% salicylic acid and 5 wt% sodium citrate was added, followed by 1 mL NaClO solution (0.05 M) and 0.2 mL of an aqueous solution of sodium nitroferricyanide (1 wt%) were added. After standing at room temperature for 2 h, the UV-Vis absorption spectrum was collected at a wavelength of 655 nm. The concentration-absorbance curve was calibrated using standard NH_4Cl solution for a series of concentrations.

The fitting curve shows good linear relation of absorbance value with NH_4Cl concentration by three times independent calibration tests.

Determination of hydrazine concentration using the Watt and Chrisp method[2]

The production of N_2H_4 in the electrolyte was estimated by the Watt and Chrisp method. The mixture of p-dimethylaminobenzaldehyde (5.99 g), concentrated HCl (30 mL) and ethanol (300 mL) was used as a color reagent. Then 2 mL above prepared reagent was mixed with 2mL of sample solution, and stirred 15 min at room

temperature. Absorbance of the resulting solution was measured at 470 nm. The concentration-absorbance curve was calibrated using standard N_2H_4 solution for a series of concentrations.

The fitting curve shows good linear relation of absorbance value with N_2H_4 concentration by three times independent calibration tests.

Calculation of Faradaic efficiency (FE) and NH_3 formation rate

The FE for NRR was defined as the amount of electric charge used for producing NH_3 divided by the total charge passing through the electrodes during the electrolysis. Assuming three electrons were needed to produce one NH_3 molecule, the FE was calculated according to the following equation:

$$FE = 3 \times F \times C_{NH4Cl} \times V / (53.5 \times Q)$$

The yield rate of NH_3 was calculated using the following equation:

$$NH_3 \text{ yield rate} = 0.318 \times C_{NH4Cl} \times V / (m_{cat} \times t)$$

Where **F** is Faraday constant (96485 C mol^{-1}), $\mathbf{C_{NH4Cl}}$ is the measured mass concentration of NH_4Cl; **V** is the volume of the cathodic reaction electrolyte; **Q** is the quantity of applied charge/electricity; **t** is the time for which the potential was applied; $\mathbf{m_{cat}}$ is the mass of catalyst loaded at the carbon cloth.

DFT calculations

Spin-polarized density functional theory (DFT) calculations were conducted using the Vienna Ab initio Simulation Package (VASP)[3, 4]. The projector augmented wave (PAW) method was used to describe electron-ion interactions. A generalized gradient approximation (GGA) used the exchange-correlational function of Perdew–Burke–Ernzernhof (PBE) with DFT+U correction (U = 5.3). The DFT-D3 empirical correction method was employed to describe van der Waals interactions[5]. Herein, the (400) plane of FeOOH was chosen as the computational model(mp-1237867, Materials Project). According to the results of EDS and ICP measurement, reasonable amounts of Mo and S atoms selectively replace the original Fe sites and hydroxyl groups in FeOOH cell. The cutoff energy for the plane-wave basis was set as 400 eV,

and the total energy convergence was set to be lower than 1×10^{-5} eV, with the force convergence set at 0.05 eV/Å for geometric optimizations. A Monkhorst-Pack k-points setting of $2 \times 3 \times 1$ and $3 \times 4 \times 1$ were used to sample the Brillouin zone for geometry optimizations and electronic structure computations, respectively. The adsorption energy (E_{ads}) of adsorbate was defined as $E_{ads} = E - E_{slab} - E^*$, where E, E_{slab}, and E* are total energies of catalyst with adsorbates, the isolate catalyst, and the corresponding adsorbates, respectively[6]. In addition, the free energy of the electrochemical steps of the reaction was calculated based on the computational hydrogen electrode (CHE) model. The free energies of species were calculated as $G = E_{DFT} + E_{ZPE} - T\Delta S$, where E_{DFT} was obtained from DFT energy, $E_{ZPE,}$ and $T\Delta S$ of adsorbed species were calculated by vibration analysis, whereas the thermodynamic corrections for gas molecules were from the standard database.

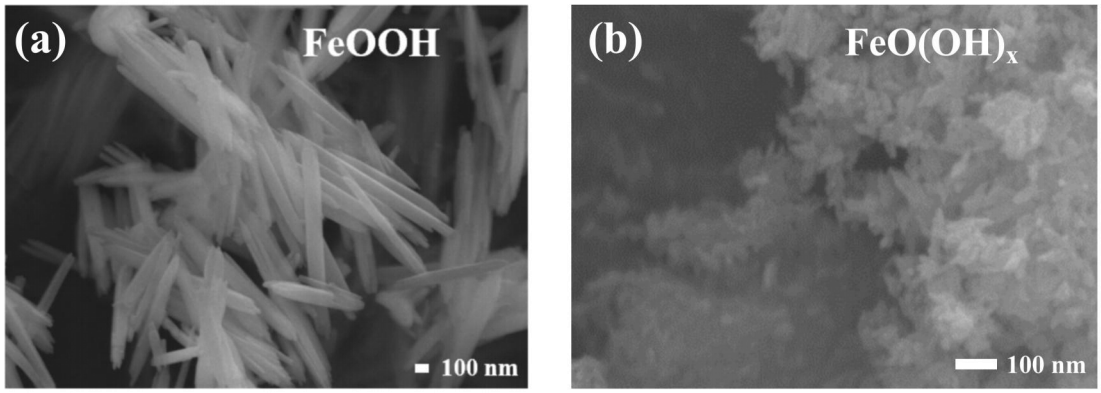

Figure S1. SEM images of pristine FeOOH (a) and $FeO(OH)_x$ (b) samples.

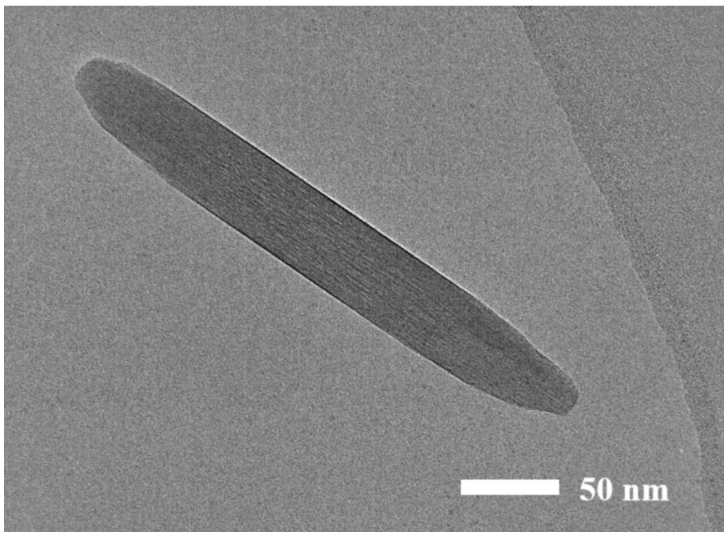

Figure S2. TEM image of FeO(OH, S) sample.

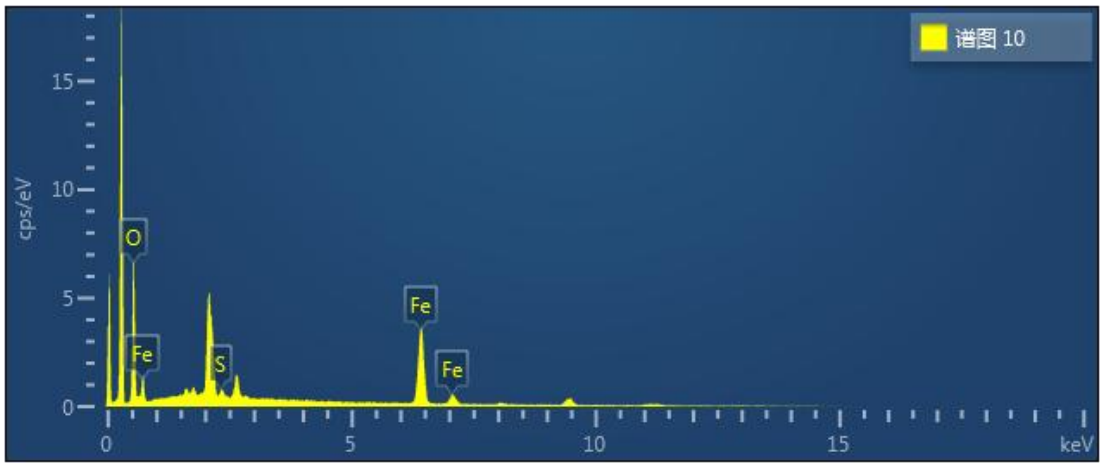

Figure S3. Elemental characteristic peaks of FeO(OH, S) sample by EDS analysis.

Table S1. The content of element in FeO(OH, S) by EDS analysis.

Elements	Mass fraction（wt%）
Fe	76.42 %
O	21.99 %
S	1.60 %

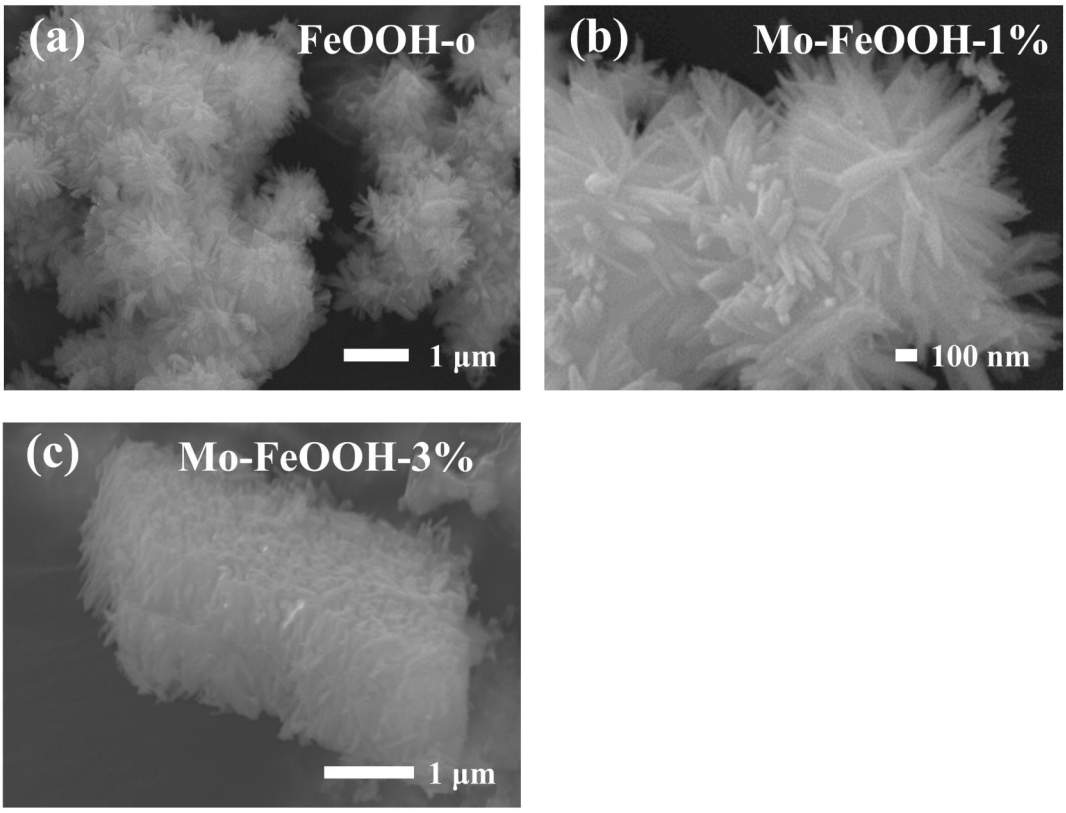

Figure S4. SEM images of FeOOH-o (a) , Mo-FeOOH (1 %) (b) and Mo-FeOOH (3 %) (c) samples.

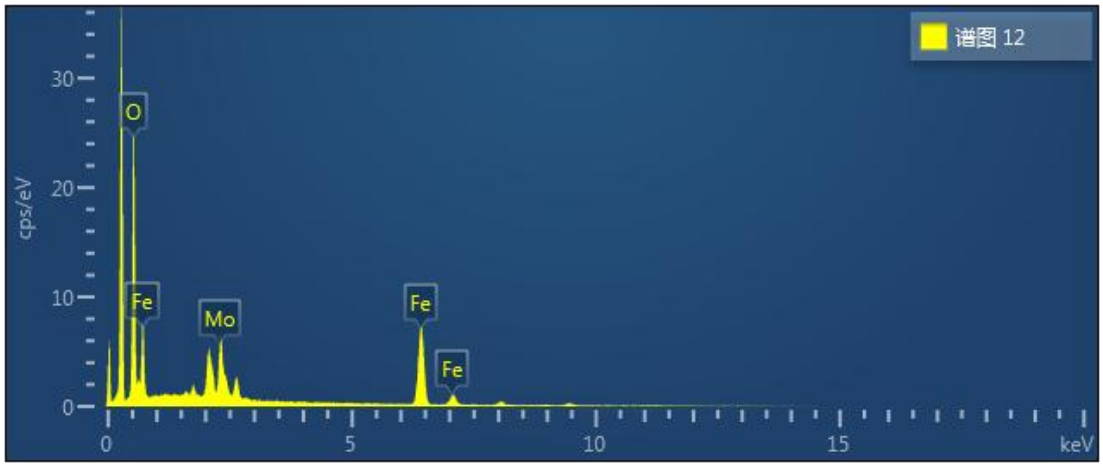

Figure S5. Elemental characteristic peaks of Mo-FeOOH sample by EDS analysis.

Table S2. The content of element in Mo-FeOOH by EDS analysis.

Elements	**Mass fraction（wt%）**
Fe	47.08 %
O	36.32 %
Mo	16.60 %

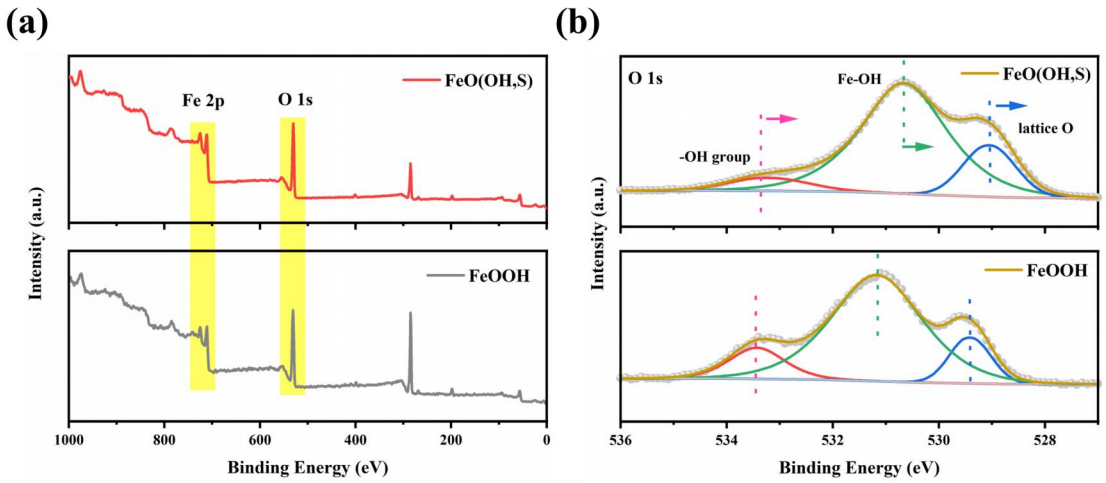

Figure S6. (a) XPS survey spectra of pristine FeOOH and FeO(OH, S) catalysts; (b) High-resolution O 1s spectra of pristine FeOOH and FeO(OH, S) catalysts.

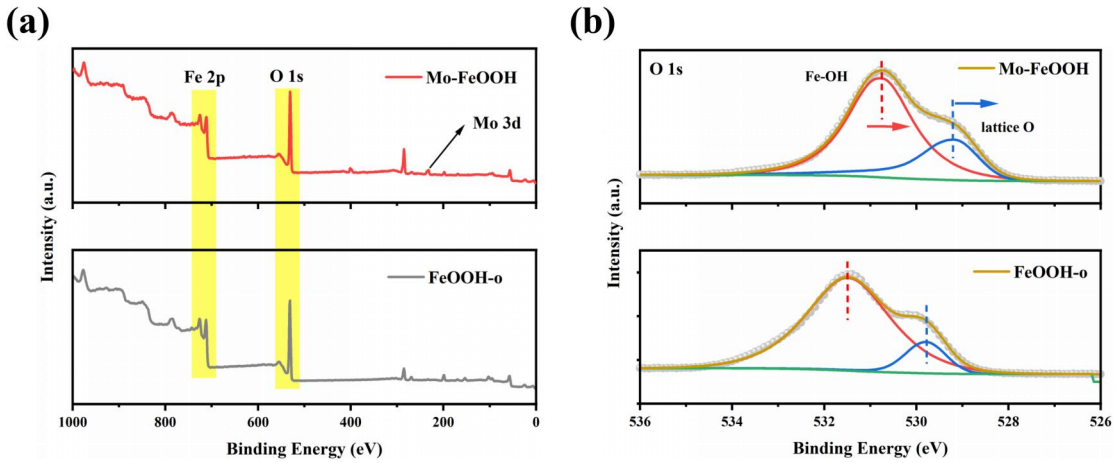

Figure S7. (a) XPS survey spectra of FeOOH-o and Mo-FeOOH catalysts; (b) High-resolution O 1s spectra of FeOOH-o and Mo-FeOOH catalysts.

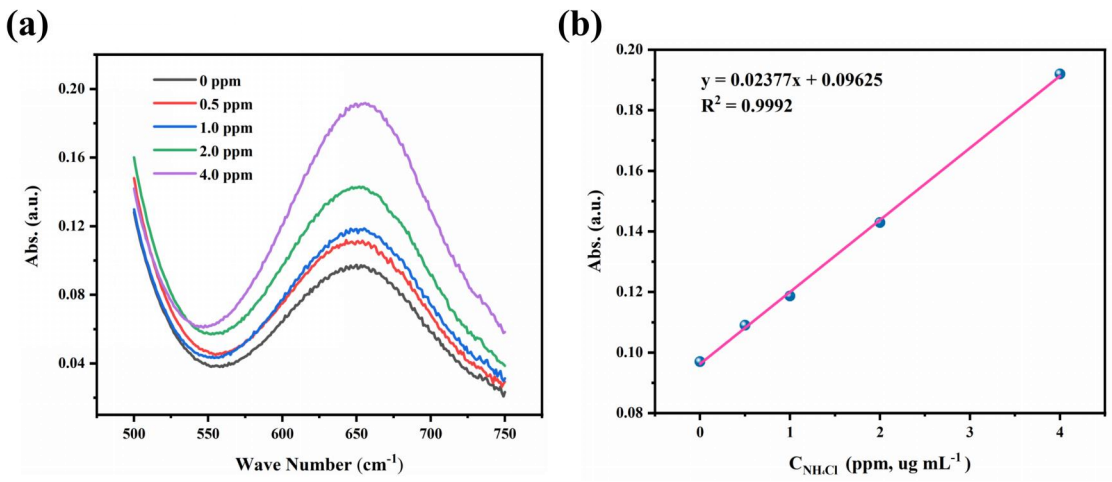

Figure S8. UV-vis curves (a) and concentration-absorbance curve (b) of NH_4Cl solution with a series of standard concentration (0 - 4 μg mL^{-1}) in 0.1 M $LiClO_4$ + 20 % PEG. The standard curve shown good linear relation of absorbance with NH_4Cl concentration (y = 0.02377x + 0.09625, R^2 = 0.9992). The absorbance at 655 nm was measured by UV-vis spectrophotometer.

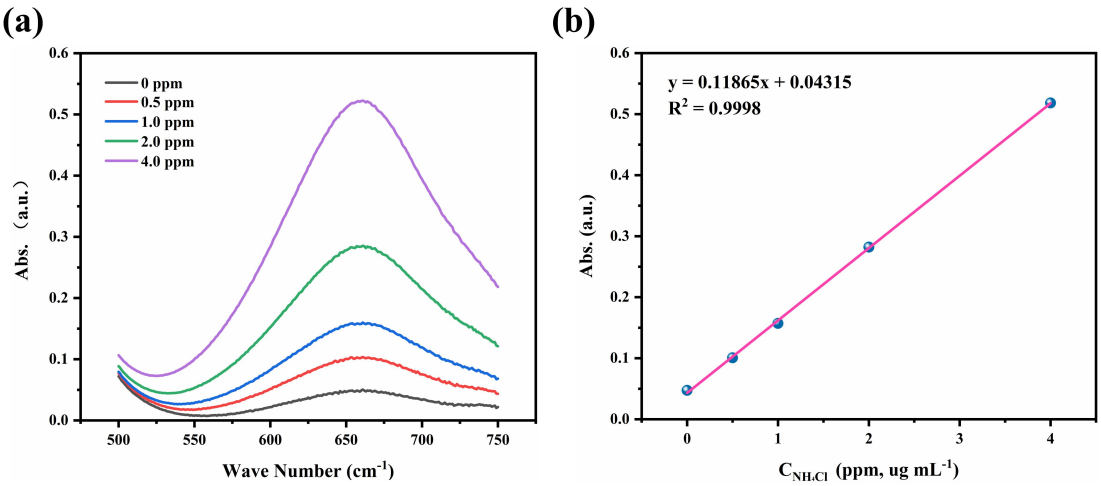

Figure S9. UV-vis curves(a) and concentration-absorbance(b) of NH_4Cl solution with a series of standard concentration (0-4 μg mL^{-1}) in 0.1 M $LiClO_4$. The standard curve shown good linear relation of absorbance with NH_4Cl concentration (y=0.11865x+0.04315, R^2=0.9998). The absorbance at 655 nm was measured by UV-vis spectrophotometer.

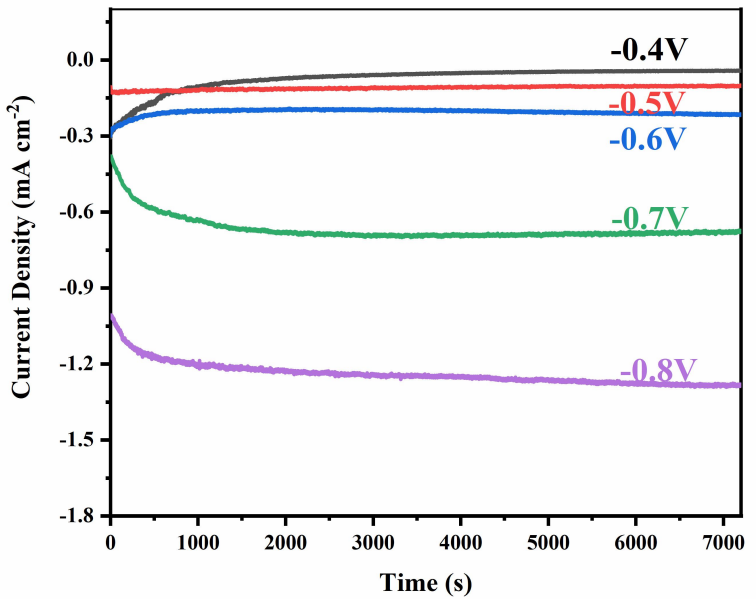

Figure S10. The chronoamperometric curves of FeO(OH, S) catalyst at various potentials for 2 h.

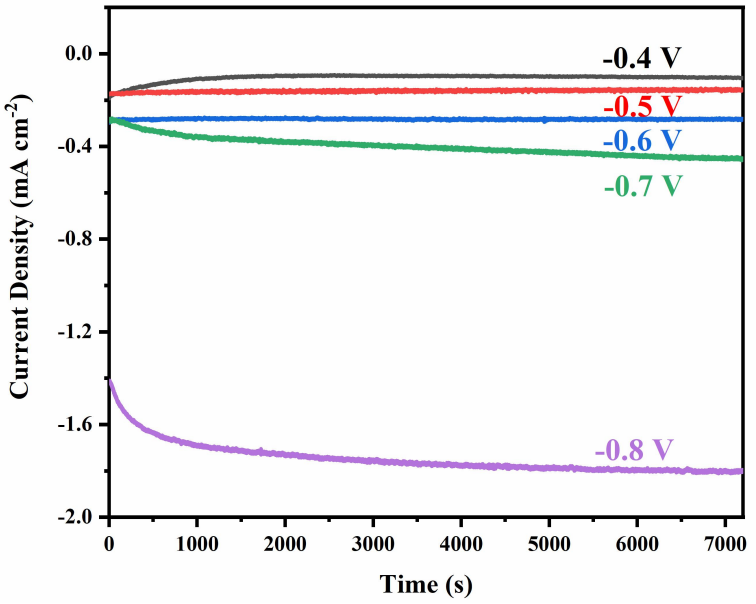

Figure S11. The chronoamperometric curves of Mo-FeOOH catalyst at various potentials for 2 h.

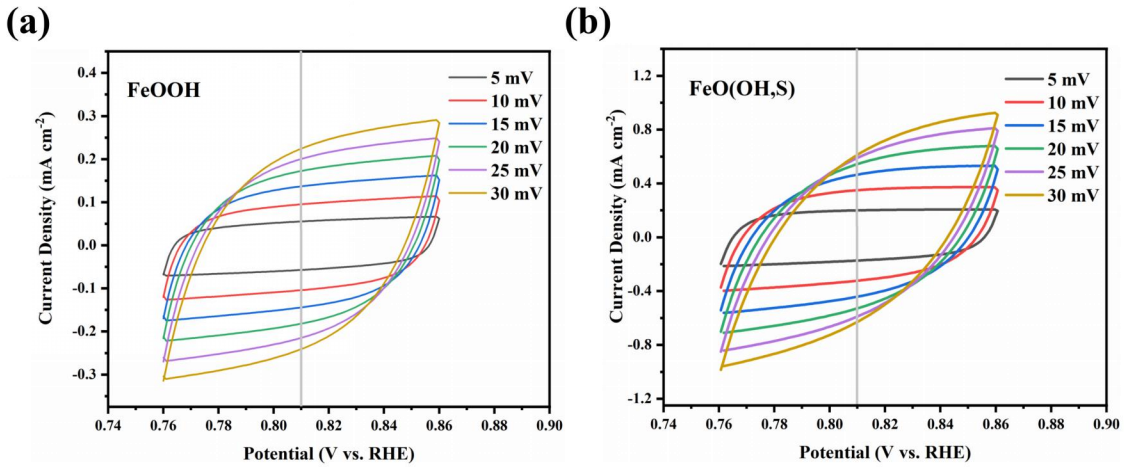

Figure S12. CV curves of (a) pristine FeOOH; (b) FeO(OH, S) catalysts with different scan rates.

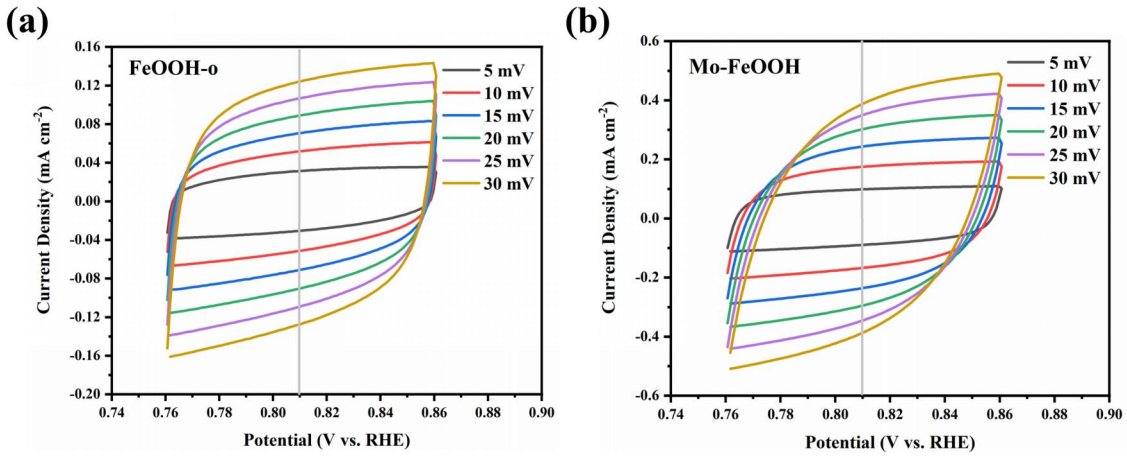

Figure S13. CV curves of (a) FeOOH-o; (b) Mo-FeOOH catalysts with different scan rates.

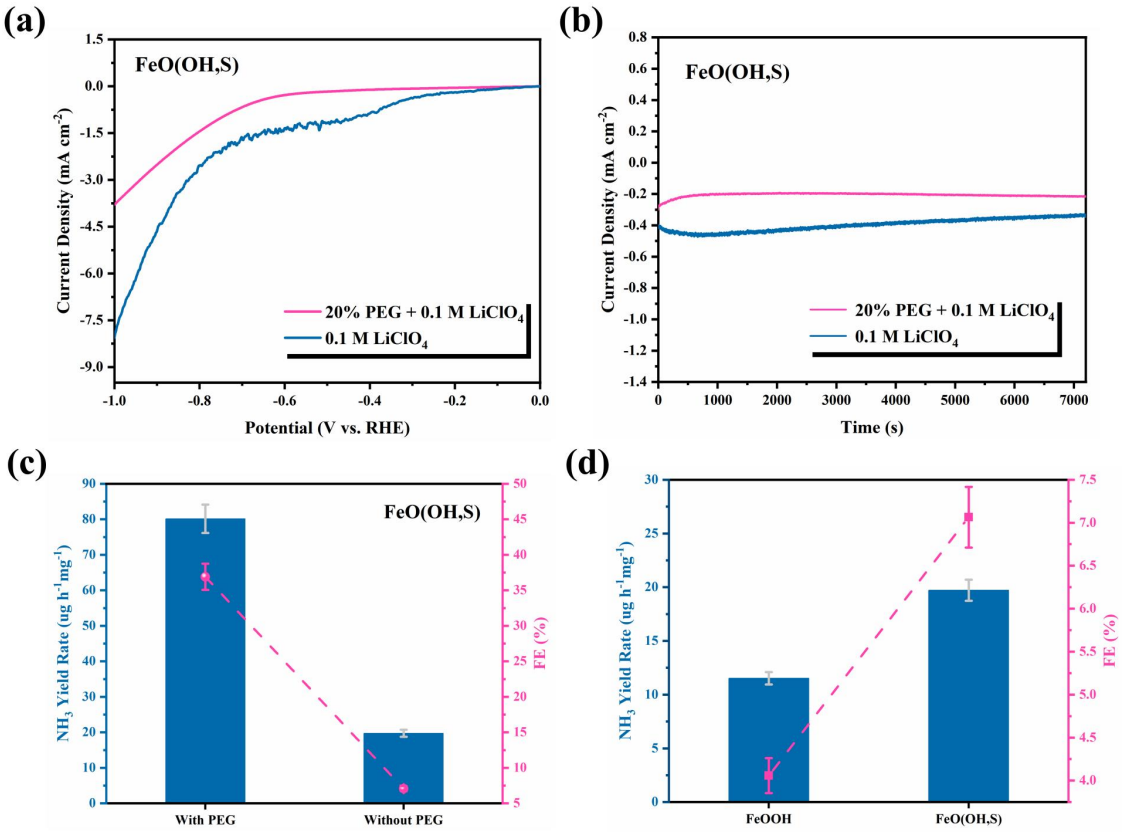

Figure S14. (a) The LSV of FeO(OH, S) catalyst in N_2 saturated electrolyte with different content of PEG; (b) The chronoamperometric curves of FeO(OH, S) catalyst at -0.6 V vs. RHE for 2 h with different content of PEG; (c) The ammonia yield rate and Faradic efficiencies of FeO(OH, S) catalyst at -0.6 V vs. RHE in N_2 saturated electrolyte with different content of PEG; (d) The ammonia yield rate of pristine FeOOH and FeO(OH, S) catalysts.

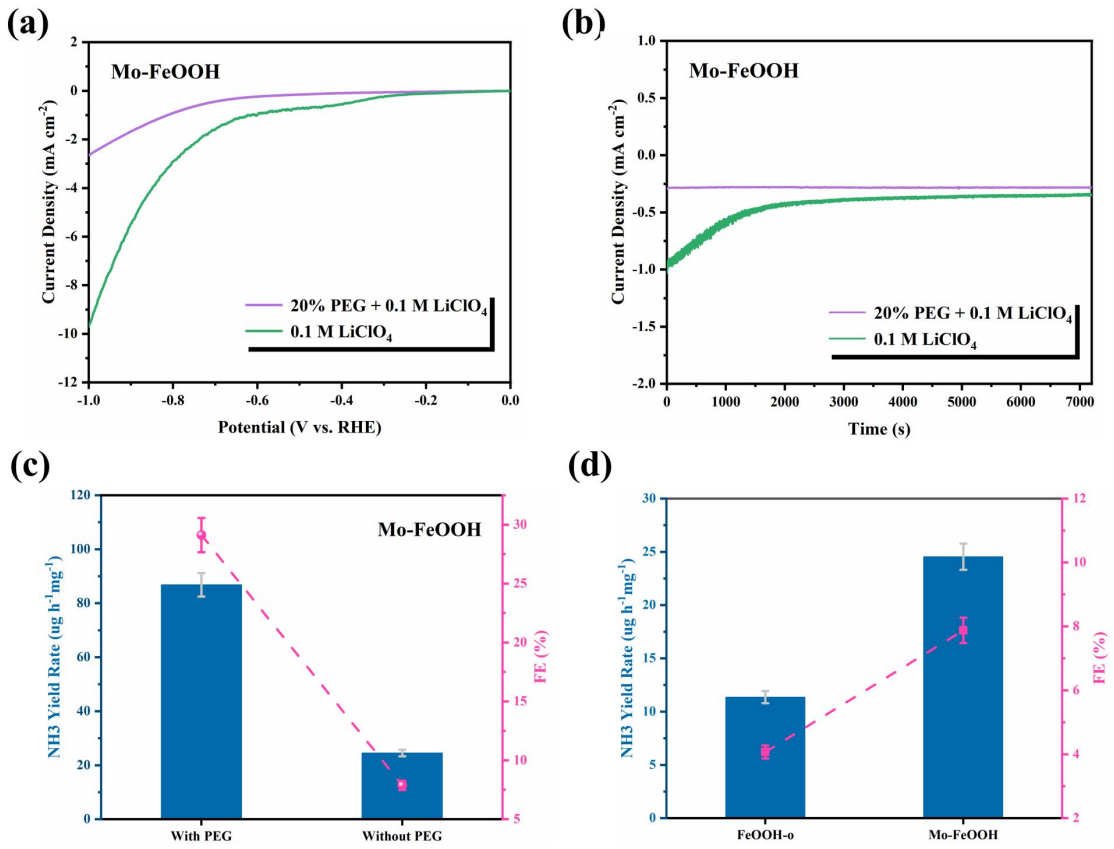

Figure S15. (a) The LSV of Mo-FeOOH catalyst in N_2 saturated electrolyte with different content of PEG; (b) The chronoamperometric curves of Mo-FeOOH catalyst at -0.6 V vs. RHE for 2 h with different content of PEG; (c) The ammonia yield rate and Faradic efficiencies of Mo-FeOOH catalyst at -0.6 V vs. RHE in N_2 saturated electrolyte with different content of PEG; (d) The ammonia yield rate of FeOOH-o and Mo-FeOOH catalysts.

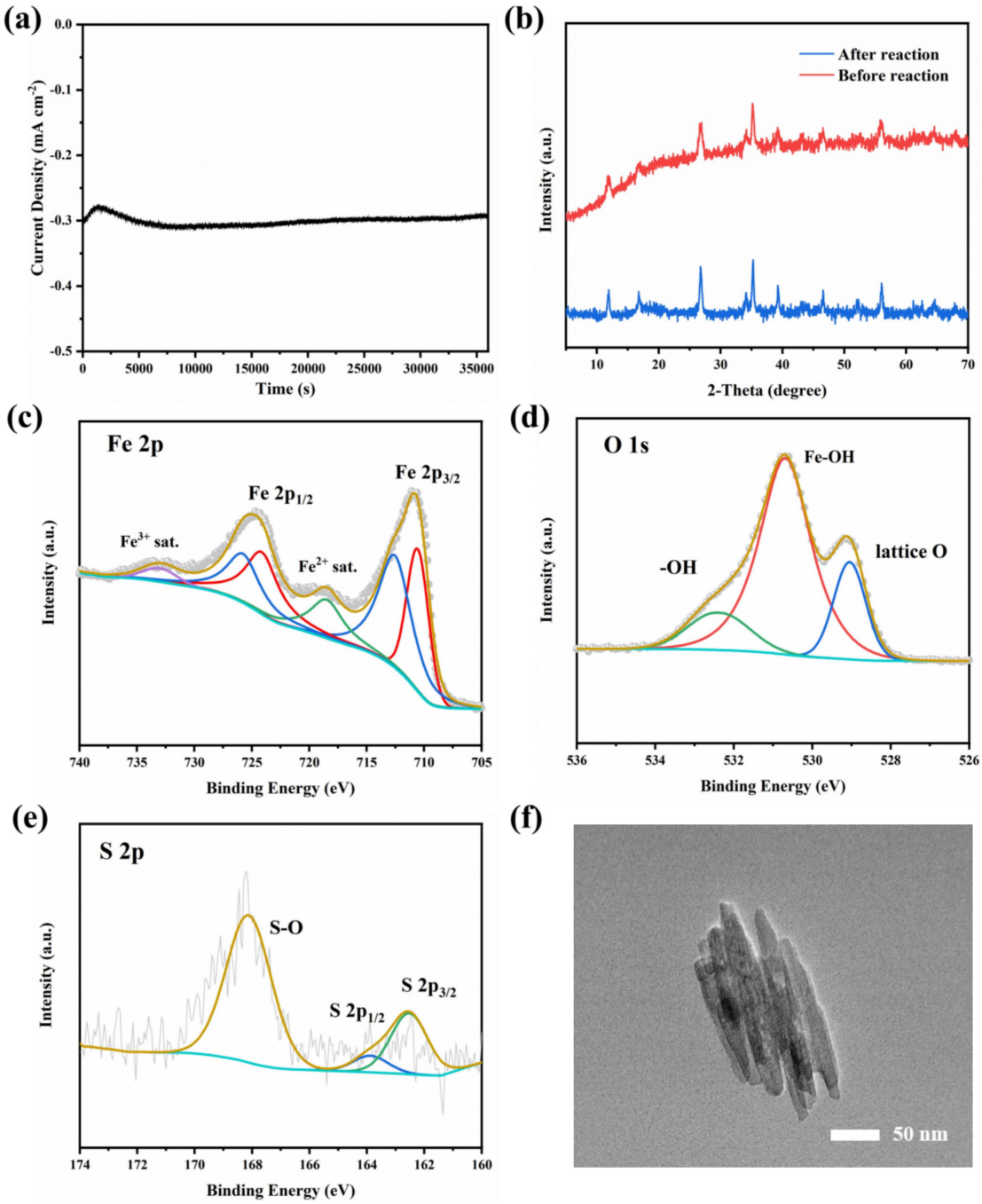

Figure S16. (a) The chronoamperometric curves of FeO(OH, S) catalyst at -0.6 V vs. RHE for 10 h in N_2 saturated 0.1 M $LiClO_4$ + 20 % PEG solution; (b) XRD patterns; (c) High-resolution Fe 2p spectrum; (d) High-resolution O 1s spectrum; (e) High-resolution S 2p spectrum; (e) TEM pattern of FeO(OH, S) catalyst after 10 h electrolysis.

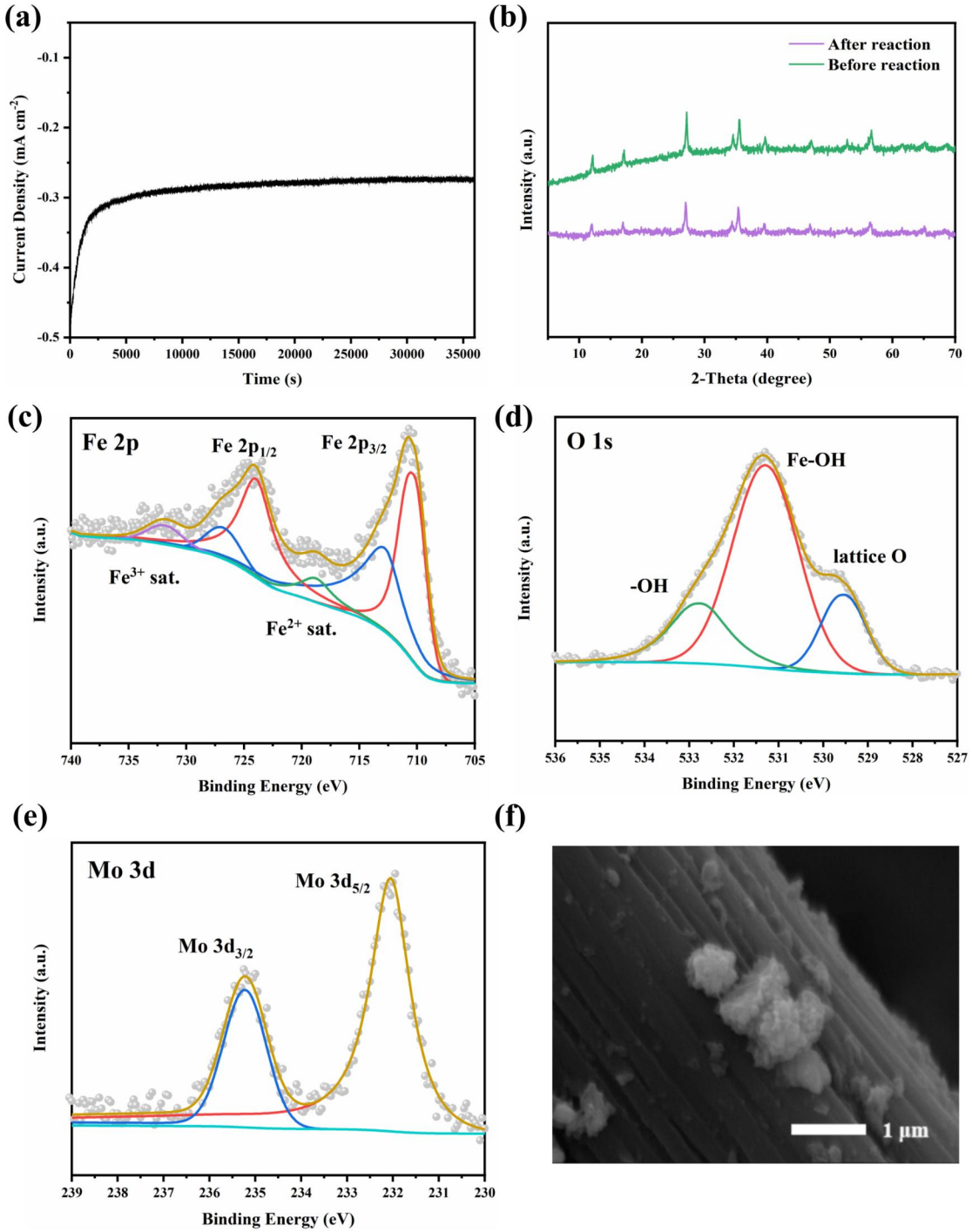

Figure S17. (a) The chronoamperometric curves of Mo-FeOOH catalyst at -0.6 V vs. RHE for 10 h in N_2 saturated 0.1 M $LiClO_4$ + 20 % PEG solution; (b) XRD patterns; (c) High-resolution Fe 2p spectrum; (d) High-resolution O 1s spectrum; (e) High-resolution Mo 3d spectrum; (e) SEM pattern of Mo-FeOOH catalyst after 10 h electrolysis.

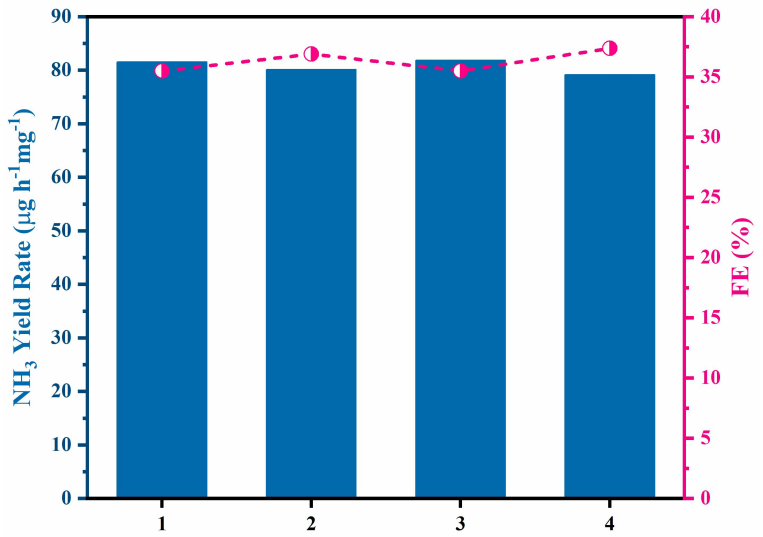

Figure S18. The Faradaic efficiency and ammonia production rate of FeO(OH, S) catalyst at -0.6 V vs. RHE during recycling tests for four times.

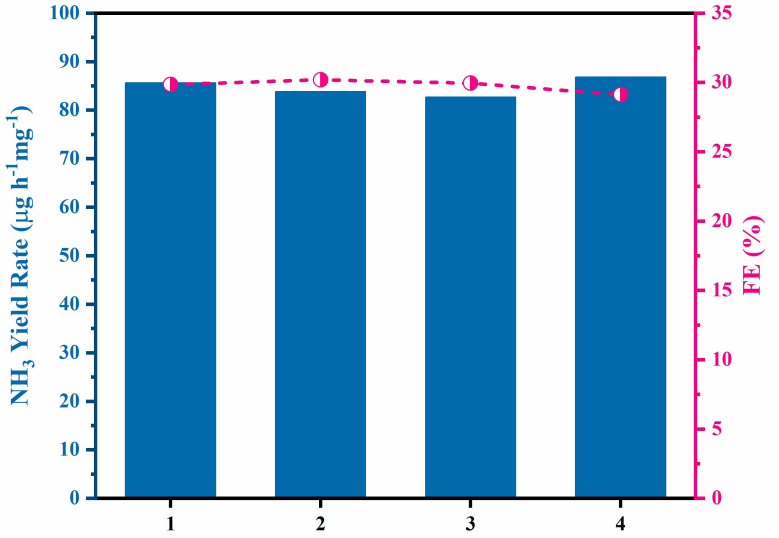

Figure S19. The Faradaic efficiency and ammonia production rate of Mo-FeOOH catalyst at -0.6 V vs. RHE during recycling tests for four times.

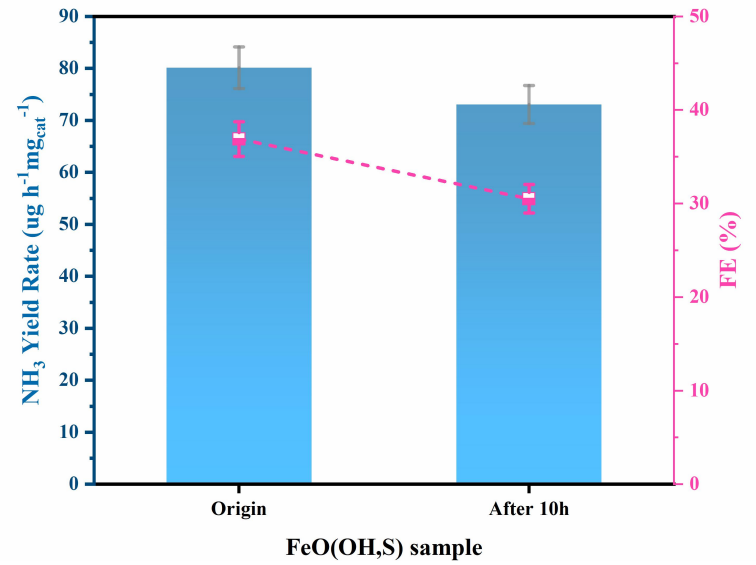

Figure S20. NH_3 production rates and FEs after long-term electrocatalytic test of 10 h for FeO(OH, S).

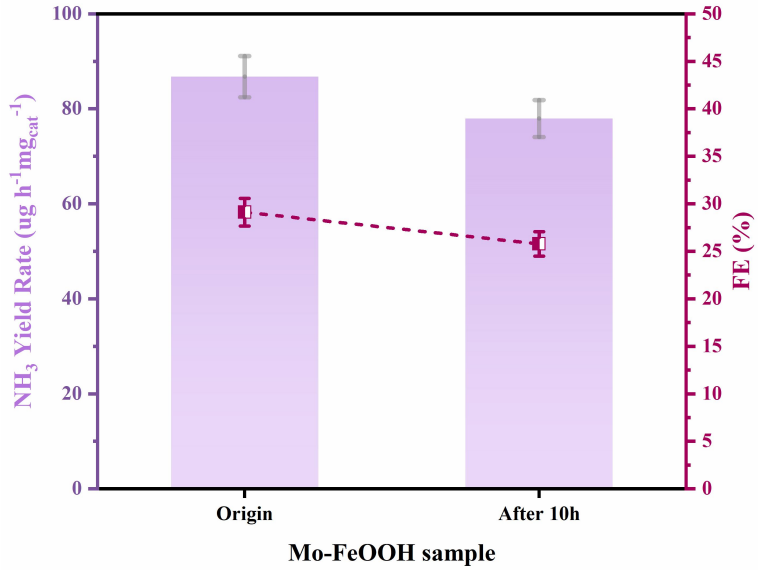

Figure S21. NH_3 production rates and FEs after long-term electrocatalytic test of 10 h for Mo-FeOOH.

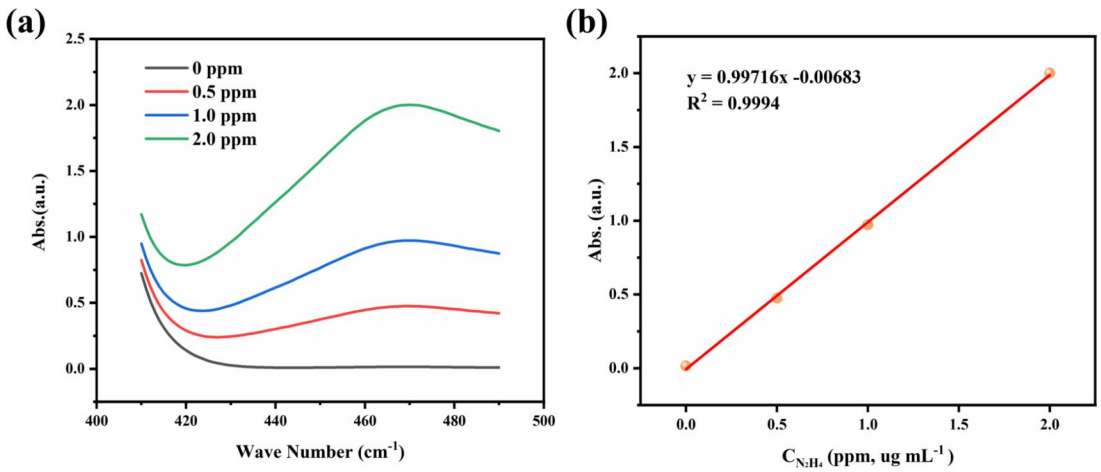

Figure S22. UV-vis curves (a) and concentration-absorbance curve (b) of N_2H_4 solution with a series of standard concentration (0 - 2 μg mL^{-1}) in 0.1 M $LiClO_4$ + 20 % PEG; The absorbance at 470 nm was measured by UV-vis spectrophotometer; The standard curve shown good linear relation of absorbance with N_2H_4 concentration (y = 0.99716x - 0.00683, R^2 = 0.9994).

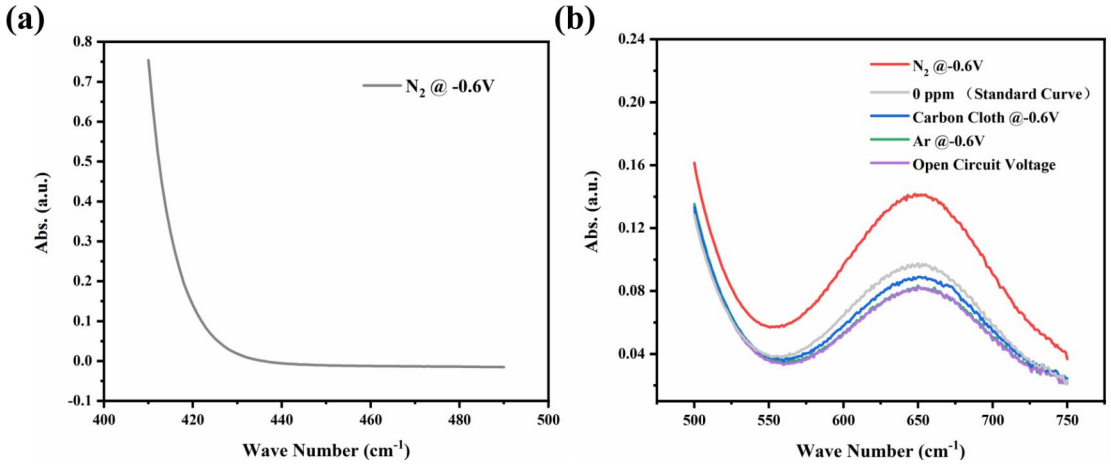

Figure S23. (a) UV-vis spectra of the electrolyte stained with N_2H_4 indicator after electrolysis 2 h in N_2-saturated solution at the potential of -0.6 V vs. RHE for FeO(OH, S) catalyst; (b) UV-vis spectra of the electrolyte stained with NH_4^+ indicator under bare carbon cloth, prepared catalyst, open circle voltage after electrolysis 2 h in N_2-saturated solution and under prepared catalyst after electrolysis 2 h in Ar-saturated solution at the potential of -0.6 V vs. RHE for FeO(OH, S) catalyst.

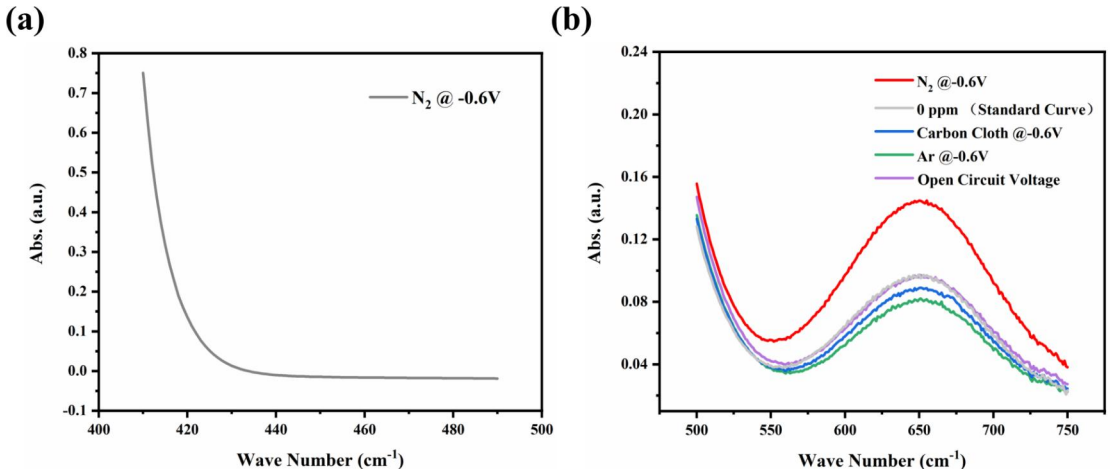

Figure S24. (a) UV-vis spectra of the electrolyte stained with N_2H_4 indicator after electrolysis 2 h in N_2-saturated solution at the potential of -0.6 V vs. RHE for Mo-FeOOH catalyst; (b) UV-vis spectra of the electrolyte stained with NH_4^+ indicator under bare carbon cloth, prepared catalyst, open circle voltage after electrolysis 2 h in N_2-saturated solution and under prepared catalyst after electrolysis 2 h in Ar-saturated solution at the potential of -0.6 V vs. RHE for Mo-FeOOH catalyst.

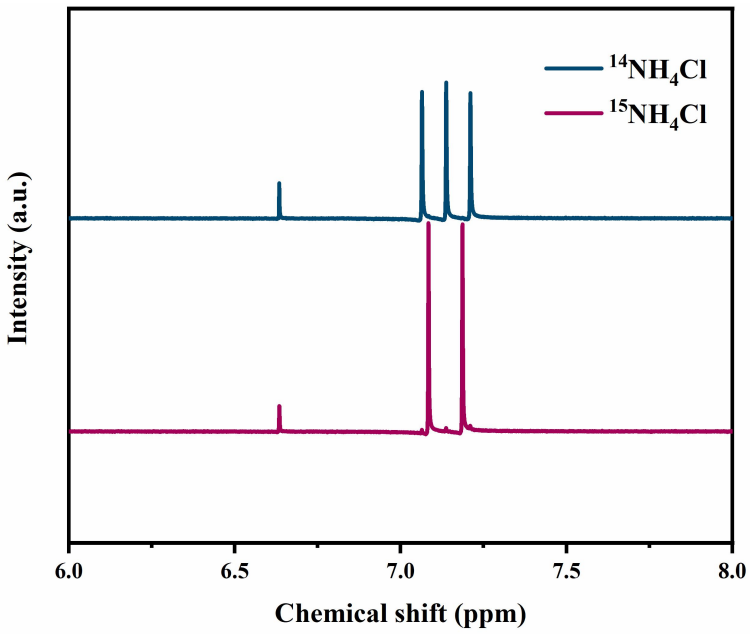

Figure S25. ^{1}H NMR spectra of standard $^{15}NH_4Cl$/ $^{14}NH_4Cl$ solution.

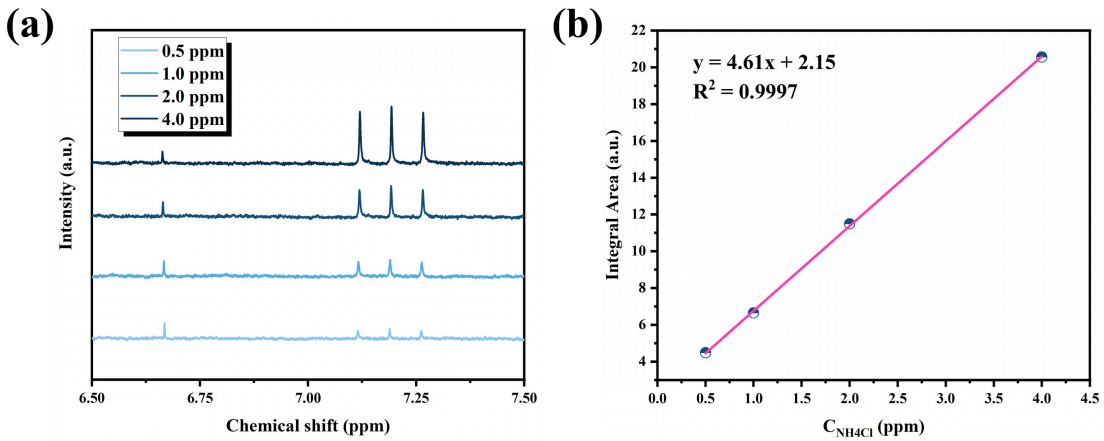

Figure S26. (a) $^{14}NH_4Cl$ solution with a series of standard concentration (0.5 - 4 μg mL^{-1}) in 0.1 M $LiClO_4$ + 20 % PEG; (b) the standard curve shown good linear relation of integral area with $^{14}NH_4Cl$ concentration (y = 4.61x + 2.15, R^2 = 0.9997).

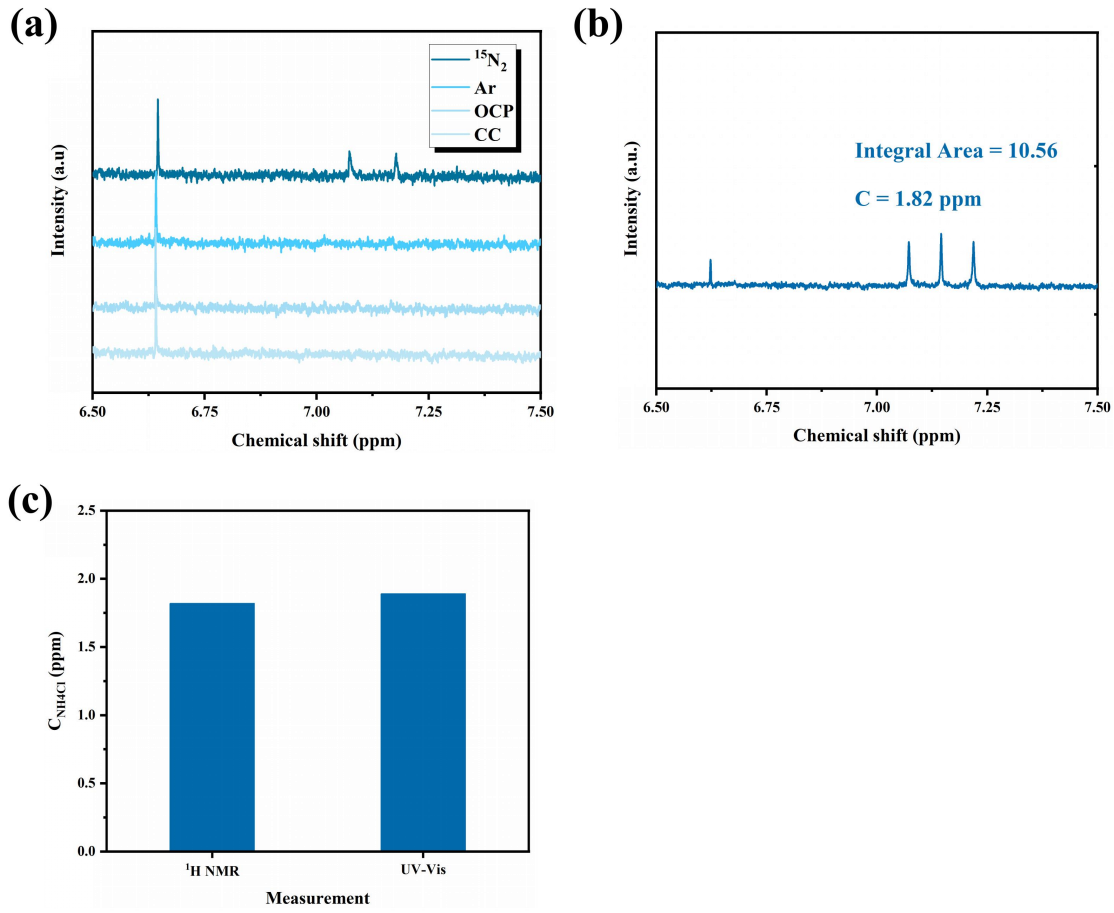

Figure S27. (a) $^{15}N_2$ and blank experiments in 0.1 M $LiClO_4$ + 20 % PEG under different situations; (b) electrolyte saturated with $^{14}N_2$ after 2 h of electrolysis; (c) the ammonia yield of FeO(OH, S) catalyst after 2 h of electrolysis determined using the UV-Vis spectrum and ^{1}H NMR spectra.

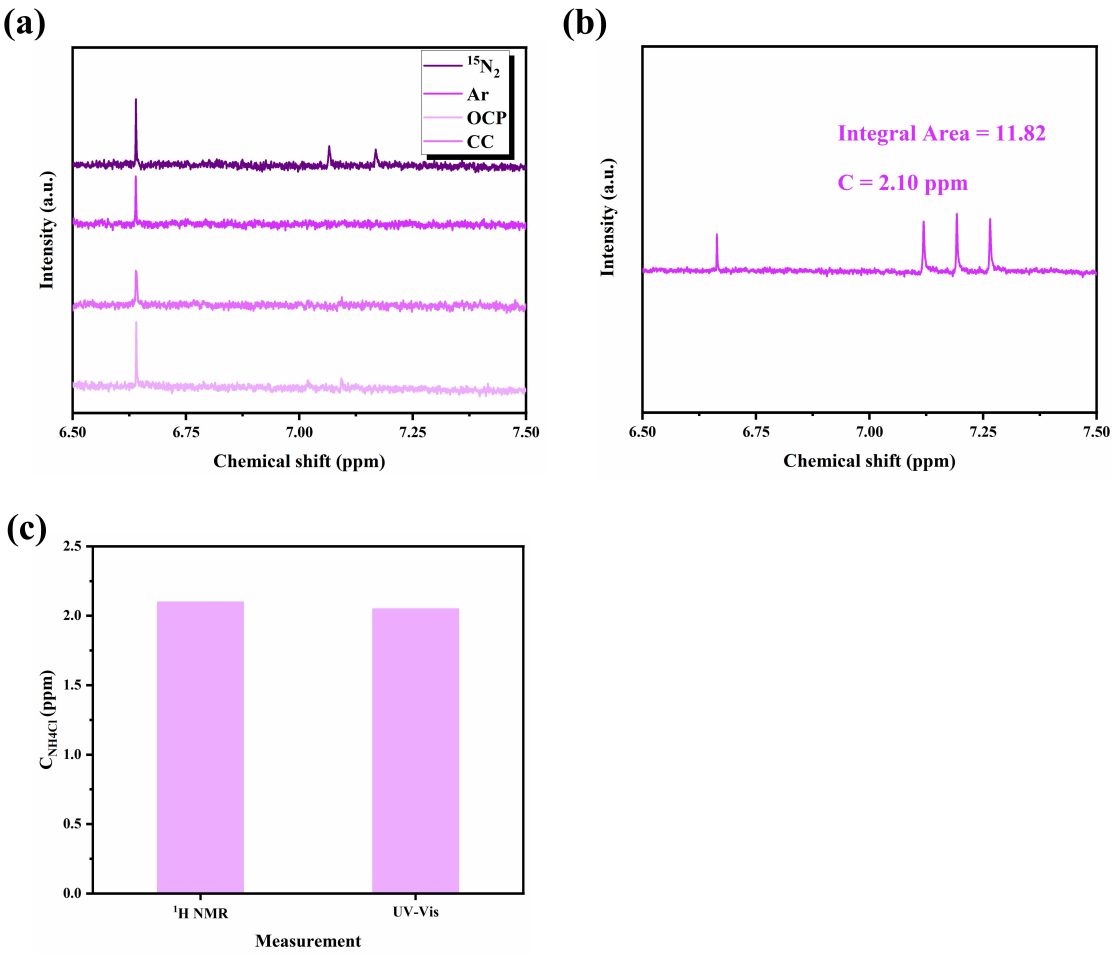

Figure S28. (a) $^{15}N_2$ and blank experiments in 0.1 M $LiClO_4$ + 20 % PEG under different situations; (b) electrolyte saturated with $^{14}N_2$ after 2 h of electrolysis; (c) the ammonia yield of Mo-FeOOH catalyst after 2 h of electrolysis determined using the UV-Vis spectrum and ^{1}H NMR spectra.

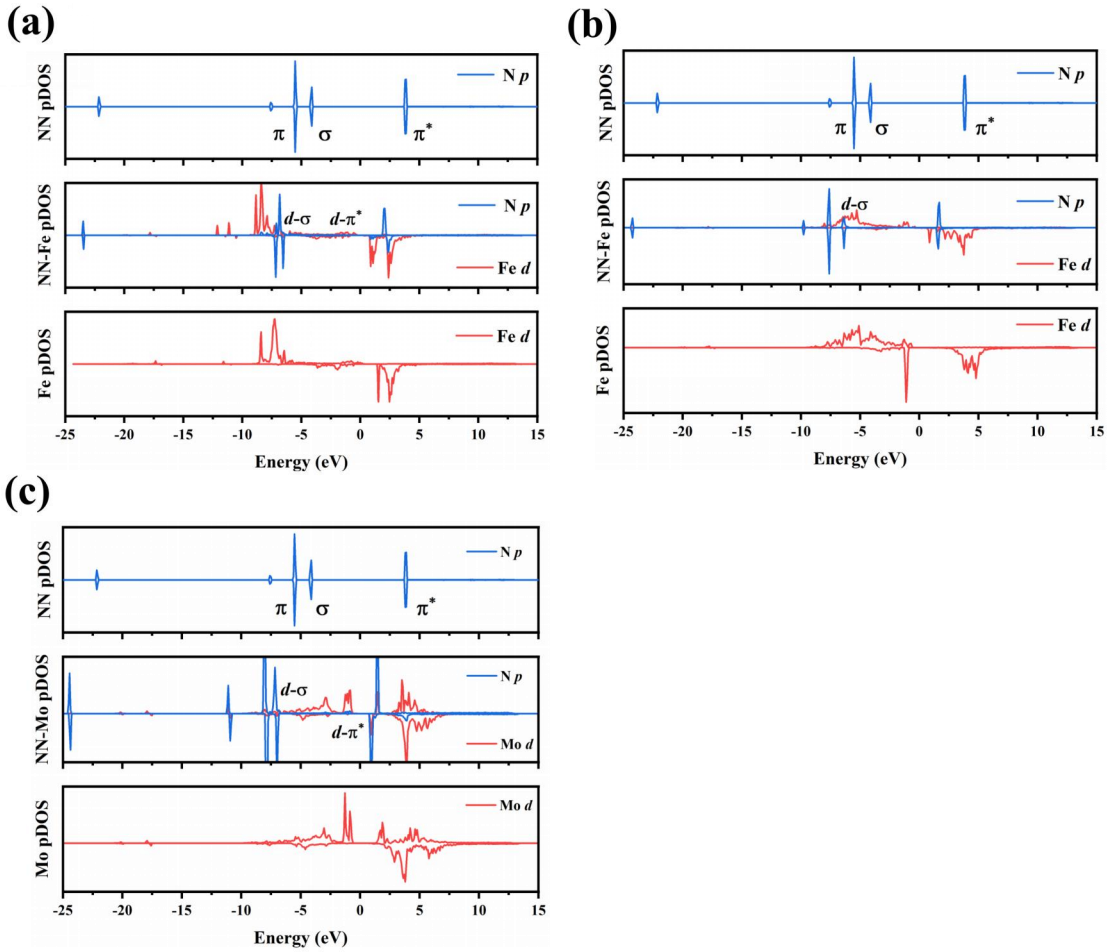

Figure S29. (a) The pDOS of N_2 adsorbed at Fe sites from FeO(OH, S); (b) The pDOS of N_2 adsorbed at Fe sites from Mo-FeOOH catalyst; (c) The pDOS of N_2 adsorbed at Mo sites from Mo-FeOOH catalyst.

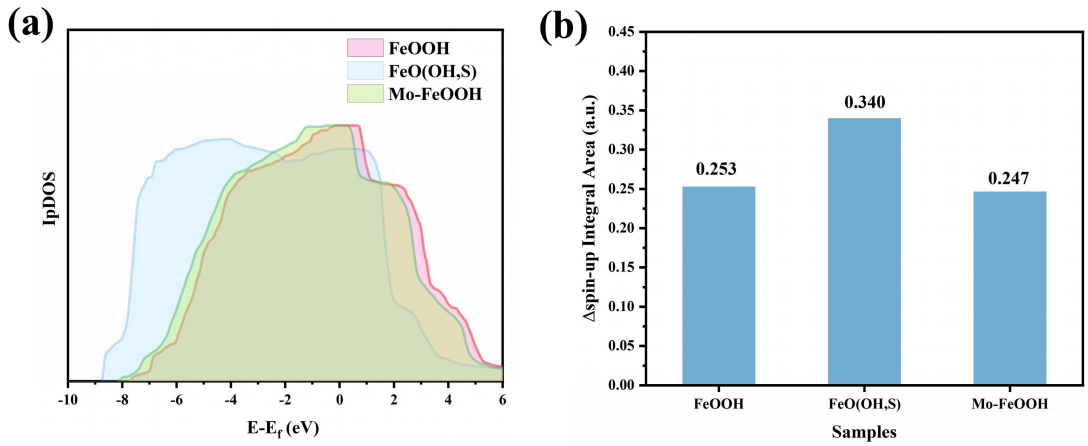

Figure S30. The net spin up (Δspin-up) of Fe sites in pristine FeOOH, FeO(OH, S) and Mo-FeOOH species (a) and corresponding integral area (b).

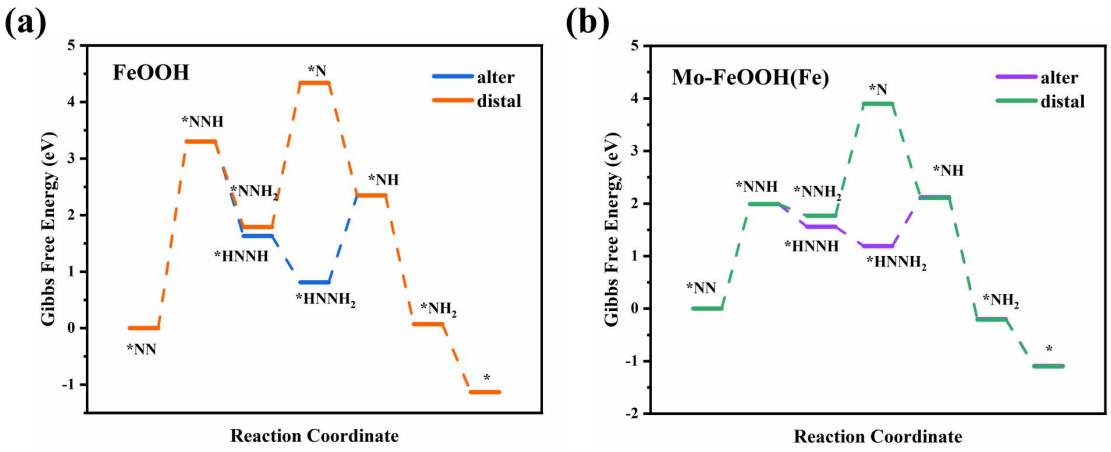

Figure S31. The Gibbs energy of electrolytic ammonia production over FeOOH (a) and Mo-FeOOH(Fe) samples.

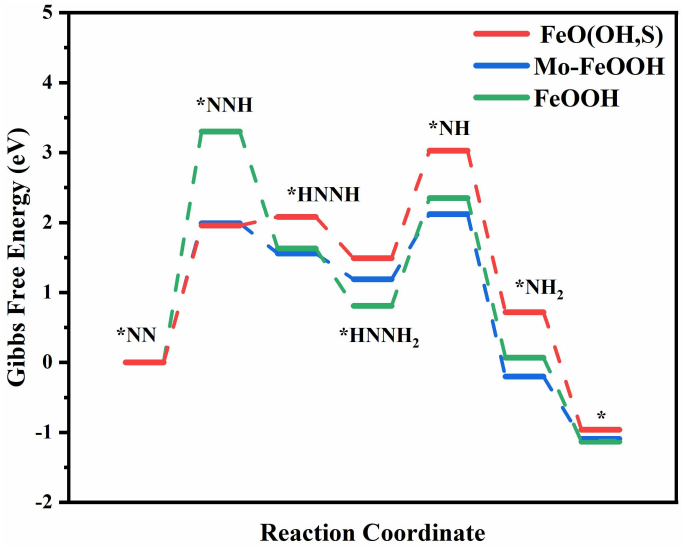

Figure S32. The Gibbs energy of electrolytic ammonia production over FeOOH, FeO(OH, S) and Mo-FeOOH samples in alter-pathway.

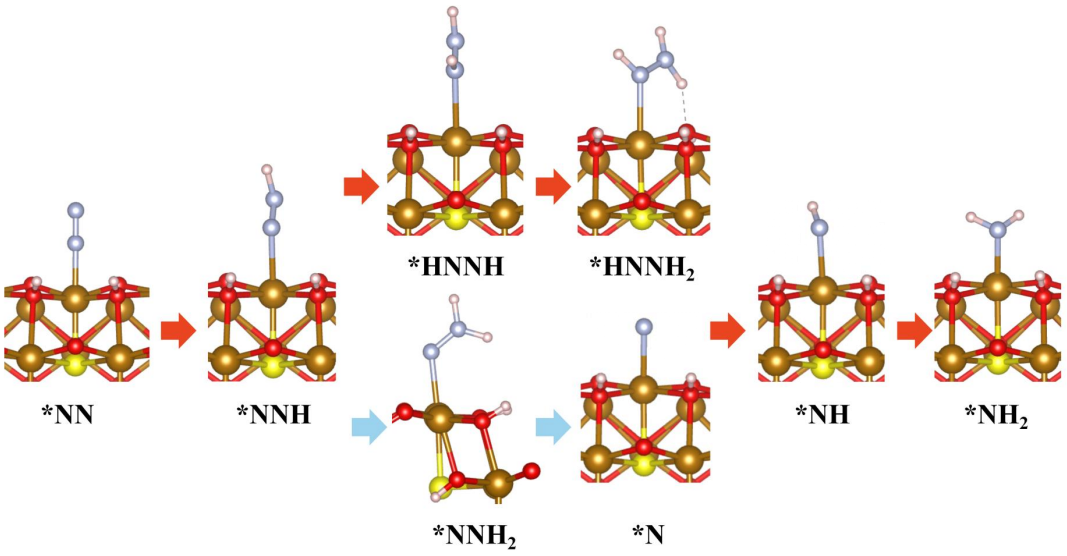

Figure S33. The adsorption configuration for each intermediate on the surface of FeO(OH, S).

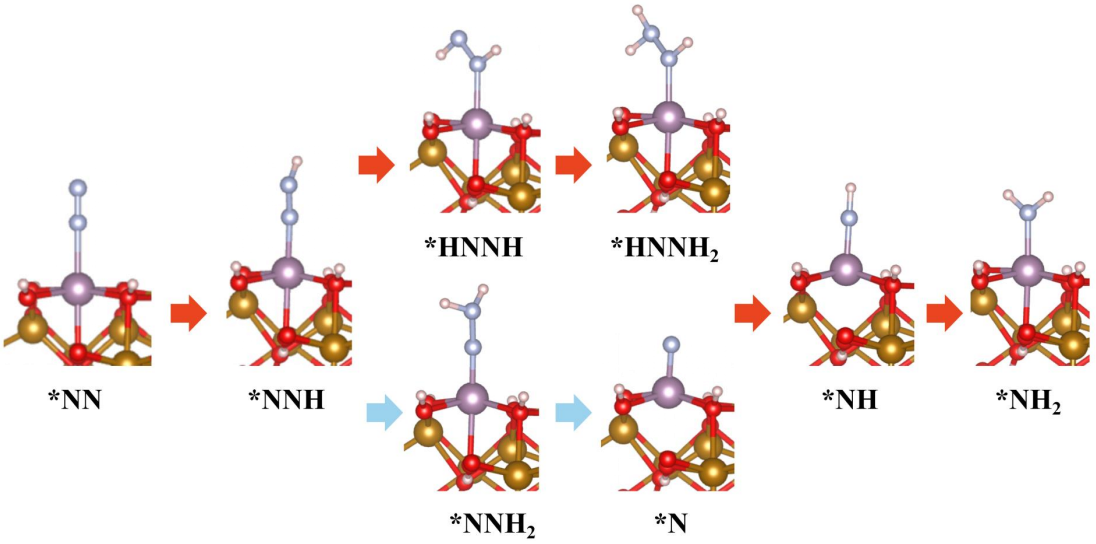

Figure S34. The adsorption configuration for each intermediate on the surface of Mo-FeOOH.

Table S3. Comparison of the electrocatalytic activity of FeOOH-T to produce ammonia with previously reported studies

Catalyst	Electrolyte	NH_3 Yield	FE
β-FeOOH[7]	0.5 M $LiClO_4$	23.32 μg h^{-1} mg_{cat}^{-1}	6.7 %
FeO(OH,F)[8]	0.5 M $LiClO_4$	42.38 μg h^{-1} mg_{cat}^{-1}	9.02 %
FeOOH QDs/Graphene[9]	0.1 M $LiClO_4$	27.3 μg h^{-1} mg_{cat}^{-1}	14.6 %
Zr-α-FeOOH[10]	0.1 M Na_2SO_4	1.39×10^{-10} mol $s^{-1}cm^{-2}$	35.63 %
TiO_2[11]	0.05 M H_2SO_4 + PEG	1.07 μmol $cm^{-2}h^{-1}$	32.13 %
Cu-HEX[12]	0.1 M KOH	1.2 μg h^{-1} cm^{-2}	50.5 %
$Au/Fe_2(MoO_4)_3$[13]	0.2 m Na_2SO_4	7.61 μg h^{-1} mg_{cat}^{-1}	18.79 %
F-Fe: TiO_2[14]	0.05 M H_2SO_4	27.86 μg h^{-1} mg_{cat}^{-1}	27.67 %
FeMo/NC[15]	0.1 M Na_2SO_4	26.8 μg h^{-1} mg_{cat}^{-1}	11.8 %
Fe-B/N-C[16]	0.1 M KOH	100.1 μg h^{-1} mg_{cat}^{-1}	23.0 %
FeMoPPc[17]	0.1 M KOH	36.33 μg h^{-1} mg_{cat}^{-1}	20.62 %
Fe_{SA}-NO-C[18]	0.1 M HCl	31.9 μg h^{-1} mg_{cat}^{-1}	11.8 %
D-FeN/C[19]	0.1 M KOH	24.8 μg h^{-1} mg_{cat}^{-1}	15.8 %
Mo-Fe_2O_3[20]	0.1 M Na_2SO_4	21.3 μg h^{-1} mg_{cat}^{-1}	11.2 %
VS_2-350[21]	0.1 M HCl	20.29 μg h^{-1} mg_{cat}^{-1}	3.86 %
Fe_{SA}-NSC-900[22]	0.1 M HCl	30.4 μg h^{-1} mg_{cat}^{-1}	21.9 %

Table S3. Comparison of the electrocatalytic activity of FeOOH-T to produce ammonia with previously reported studies (Continued)

Catalyst	Electrolyte	NH_3 Yield	FE
MoS_2-Vs[23]	0.1 M K_2SO_4	66.74 μg h^{-1} mg_{cat}^{-1}	14.68 %
$S_{6.23}$-$B_{8.09}$/CNFs[24]	0.5 M K_2SO_4	0.223 μmol h^{-1} cm^{-2}	22.4 %
CoS_x/CC-L[25]	0.05 M Na_2SO_4	12.2 μg h^{-1} mg_{cat}^{-1}	10.1 %
Bi_2S_{3-x}/$Ti_3C_2T_x$[26]	0.5 M $LiClO_4$	68.3 μg·$h^{-1}$$mg^{-1}$	22.5 %
Co_3O_{4-x}/GO[27]	0.1 M K_2SO_4	5.19 mmol $h^{-1}$$g^{-1}$	10.68 %
NiCo-LDH[28]	0.1 M Na_2SO_4	52.8 μg h^{-1} mg_{cat}^{-1}	11.5 %
$TiWO_3$/$SrWO_4$[29]	0.05 M H_2SO_4	11.17 μg h^{-1} cm^{-2}	13.42 %
Sn-CeO_{2-x}[30]	0.1 M HCl	41.1 μg h^{-1} mg_{cat}^{-1}	35.3 %
Ni_3Mo[31]	0.1 M Na_2SO_4	17.35 μg h^{-1} cm^{-2}	8.94 %
Fe–Ru CNS[32]	0.1 M Na_2SO_4	43.9 μg h^{-1} mg_{cat}^{-1}	29.3 %
Bi–MoO_x @RGO[33]	0.1 M Na_2SO_4	19.93 μg h^{-1} mg_{cat}^{-1}	17.17 %
FeO(OH,S) (This work)	**0.1M $LiClO_4$ + PEG**	**80.1±4.0 μg h^{-1} mg_{cat}^{-1}**	**36.9±0.5 %**
Mo-FeOOH (This work)	**0.1M $LiClO_4$ + PEG**	**86.8±4.1 μg h^{-1} mg_{cat}^{-1}**	**29.1±0.8 %**

Reference

1. P. L. Searle, *Analyst*, 1984, **109**, 549-568.
2. G. W. Watt and J. D. Chrisp, *Analytical Chemistry*, 1952, **24**, 2006-2008.
3. G. Kresse and J. Furthmüller, *Physical Review B*, 1996, **54**, 11169-11186.
4. G. Kresse and J. Furthmüller, *Computational Materials Science*, 1996, **6**, 15-50.
5. S. Grimme, J. Antony, S. Ehrlich and H. Krieg, *The Journal of Chemical Physics*, 2010, **132**, 154104.
6. X. Yang, J. Wan, H. Zhang and Y. Wang, *Chemical Science*, 2022, **13**, 11030-11037.
7. X. Zhu, Z. Liu, Q. Liu, Y. Luo, X. Shi, A. M. Asiri, Y. Wu and X. Sun, *Chemical Communications*, 2018, **54**, 11332-11335.
8. X. Zhu, Z. Liu, H. Wang, R. Zhao, H. Chen, T. Wang, F. Wang, Y. Luo, Y. Wu and X. Sun, *Chemical Communications*, 2019, **55**, 3987-3990.
9. X. Zhu, J. Zhao, L. Ji, T. Wu, T. Wang, S. Gao, A. A. Alshehri, K. A. Alzahrani, Y. Luo, Y. Xiang, B. Zheng and X. Sun, *Nano Research*, 2020, **13**, 209-214.
10. J. Tan, X. He, F. Yin, X. Liang, G. Li and Z. Li, *Applied Surface Science*, 2021, **567**, 150801.
11. Y. Guo, J. Gu, R. Zhang, S. Zhang, Z. Li, Y. Zhao, Z. Huang, J. Fan, Z. Chen and C. Zhi, *Advanced Energy Materials*, 2021, **11**, 2101699.
12. C. Du, C. Qiu, Z. Fang, P. Li, Y. Gao, J. Wang and W. Chen, *Nano Energy*, 2022, **92**, 106784.
13. J. Yao, Y. Zhou, J.-M. Yan and Q. Jiang, *Advanced Energy Materials*, 2021, **11**, 2003701.
14. G. Song, R. Gao, Z. Zhao, Y. Zhang, H. Tan, H. Li, D. Wang, Z. Sun and M. Feng, *Applied Catalysis B: Environmental*, 2022, **301**, 120809.
15. W. Cui, B. Geng, X. Chu, J. He, L. Jia, X. Han, X. Wang, S. Song and H. Zhang, *Nano Research*, 2023, **16**, 5743-5749.
16. Y. Zhao, S. Zhang, C. Han, Q. Lu, Q. Fu, H. Jiang, L. Yang, Y. Xing, Q. Zheng,

J. Shen, L. Yan and X. Zhao, *Chemical Engineering Journal*, 2023, **468**, 143517.

17. Y. Wang, W. Cheng, P. Yuan, G. Yang, S. Mu, J. Liang, H. Xia, K. Guo, M. Liu, S. Zhao, G. Qu, B.-A. Lu, Y. Hu, J. Hu and J.-N. Zhang, *Advanced Science*, 2021, **8**, 2102915.
18. J. Zhang, S. Geng, R. Li, X. Zhang, Y. Zhou, T. Yu, Y. Wang, S. Song and Z. Shao, *Chemical Engineering Journal*, 2021, **420**, 130492.
19. Y. Kong, L. Wu, X. Yang, Y. Li, S. Zheng, B. Yang, Z. Li, Q. Zhang, S. Zhou, L. Lei, G. Wu and Y. Hou, *Advanced Functional Materials*, 2022, **32**, 2205409.
20. Z.-Y. Niu, L. Jiao, T. Zhang, X.-M. Zhao, X.-F. Wang, Z. Tan, L.-Z. Liu, S. Chen and X.-Z. Song, *ACS Applied Materials & Interfaces*, 2022, **14**, 55559-55567.
21. L. Zhao, Y. Xiong, X. Wang, R. Zhao, X. Chi, Y. Zhou, H. Wang, Z. Yang and Y.-M. Yan, *Small*, 2022, **18**, 2106939.
22. Y. Li, Y. Ji, Y. Zhao, J. Chen, S. Zheng, X. Sang, B. Yang, Z. Li, L. Lei, Z. Wen, X. Feng and Y. Hou, *Advanced Materials*, 2022, **34**, 2202240.
23. H. Fei, R. Liu, J. Wang, T. Guo, Z. Wu, D. Wang and F. Liu, *Advanced Functional Materials*, **n/a**, 2302501.
24. Y. Wen, H. Zhu, J. Hao, S. Lu, W. Zong, F. Lai, P. Ma, W. Dong, T. Liu and M. Du, *Applied Catalysis B: Environmental*, 2021, **292**, 120144.
25. L. Zhao, B. Chang, T. Dong, H. Yuan, Y. Li, Z. Tang, Z. Liu, H. Liu, X. Zhang and W. Zhou, *Journal of Materials Chemistry A*, 2022, **10**, 20071-20079.
26. Y. Luo, P. Shen, X. Li, Y. Guo and K. Chu, *Nano Research*, 2022, **15**, 3991-3999.
27. Y. Sun, Q. Wang and Z. Liu, *ACS Applied Materials & Interfaces*, 2022, **14**, 43508-43516.
28. Z. Zou, L. Wu, F. Yang, C. Cao, Q. Meng, J. Luo, W. Zhou, Z. Tong, J. Chen, S. Chen, S. Zhou, J. Wang and S. Deng, *ChemSusChem*, 2022, **15**, e202200127.
29. K. Chen, X. Xu, Q. Mei, J. Huang, G. Yang and Q. Wang, *Applied Catalysis B:*

Environmental, 2024, **341**, 123299.

30. Y. Xiao, X. Tan, Y. Guo, J. Chen, W. He, H. Cui and C. Wang, *Journal of Energy Chemistry*, 2023, **87**, 400-407.
31. H. Y. Zhou, Y. B. Qu, Y. C. Fan, Z. L. Wang, X. Y. Lang, J. C. Li and Q. Jiang, *Applied Catalysis B: Environmental*, 2023, **339**, 123133.
32. M. Liu, S. Zhang, M. Chen, S. Zhou and L. Wu, *Journal of Materials Chemistry A*, 2023, **11**, 14900-14910.
33. Y. Wan, Z. Wang, M. Zheng, J. Li and R. Lv, *Journal of Materials Chemistry A*, 2023, **11**, 818-827.